Research article

Quantity and spatial distribution of earth-air activity in Cave 108 of the Dunhuang Mogao Grottoes

Fei Li [a], Hongshou Li [a,*], Shunren Wang [b]

[a] *Dunhuang Grottoes Monitoring Center of Dunhuang Academy, Dunhuang, 736200, China*
[b] *Gansu Mogao Grottoes Cultural Heritage Conservation and Design Consulting Co., Ltd, China*

A R T I C L E I N F O	A B S T R A C T
	Monitoring of earth-air humidity in soil has revealed extensive rising/falling activity on the land. Alternation of dry and wet air is the main root cause deterioration in cave wall paintings. However, the quantity and spatial distribution of earth-air activity in caves remain unclear. This study used air flowmeters to monitor the earth-air outflow at 136 points on the west, south, and north walls of Cave 108 in the Dunhuang Mogao Grottoes, and to determine its spatial distribution. Results showed that under the influence of atmospheric fluctuation, there is frequent air exchange between the atmosphere and the earth-air, and that the daily outflow of earth-air from Cave 108 is 50.893 m^3/d. Earth-air flux is negatively correlated with atmospheric pressure, and the fluctuation of atmospheric pressure is the main driving force of earth-air activity. The average outflow of earth-air from the ground of Cave 108 is 0.109 L/(min·m^2). Apart from that, the overall spatial distribution of earth-air quantity showed the following pattern: ground > west wall > north wall > south wall. What's more, the outflow of earth-air is inversely proportional to the wall height, while proportional to the depth of the cave embedded in the cliff. In such case, sealing the cave floor with concrete will heighten earth-air flow on the walls, thereby quickening the deterioration process of wall paintings. This study unveiled the deterioration mechanism of wall paintings in the context of earth-air conditions, thus establishing a foundation for the scientific protection of wall paintings.

1. Introduction

Earth-air refers to air in the vadose zone [1]. Earth-air and external atmospheric air form a complete continuum [2]. Earth-air activity caused by fluctuation of atmospheric pressure (AP) is known as barometric pumping [3], the rise and fall of earth-air [4, 5], or passive breathing of earth-air [6]. The present authors previous studies revealed that frequent interaction between the atmosphere and earth-air plays a key role in the vertical migration and evaporation of soil water [6,7]. Their work preliminarily determined a theoretical model of a closed system for earth-air activity. When there is increase in AP, the earth-air falls and its volume is compressed, and dry atmosphere air enters the soil, leading to a reduction in relative humidity. When AP falls, the earth-air rises and its volume increases, and wet earth-air (rising damp) flows out, resulting in an increase in relative humidity. Thus, fluctuation of AP is the main root cause of earth-air activity. Under the driving force of AP fluctuation, earth-air activity is an important means of material/energy exchange both inside and outside soil, among which the rise and fall of earth-air have important effects on water/material

---

* Corresponding author.
  E-mail address: lihongshou@dha.ac.cn (H. Li).

transport and heat transfer in the soil. Earlier research showed that this movement of earth-air has substantial impact on haze patterns [8], mines and landfills [9,10], volatile gases [11], CO_2 [12], radiation from nuclear explosions [13], transportation of gases such as SO_2 and CH_4 [14–16], noble gas migration [17,18], and ^{222}Rn [19–21].

Under the background of AP variation, earth-air activity is widespread on land [22,23]. For cultural relics in caves, the effect of alternating dry and wet conditions of the atmospheric environment can lead to repeated crystallization of salt at the interface of wall paintings, thereby changing the structure of the wall paintings and causing salt-related deterioration [24,25], the most representative example of which is efflorescence [26]. Efflorescence is commonly known as wall painting 'cancer' and once formed, it is difficult to treat [27]. It has been found that the rise and fall of earth-air activity can cause increase and reduction in humidity of environmental air in caves, which is fundamental to the occurrence of efflorescent deterioration belts near the ground in buildings, walls, and wall paintings [28].

The Dunhuang Mogao Grottoes extend to 735 caves with wall paintings covering a total area of more than 45,000 m². The Mogao Grottoes represent the world's largest, longest-lasting, richest, and best-preserved art treasure house, and they have extremely important historical, cultural, and scientific research value [29]. In recent years, in conjunction with climate change, increases in regional dust storm activity and rainfall amount have elevated the threat to the cultural relics in the Mogao Grottoes through further deterioration of cave wall paintings and widespread occurrence of efflorescence, pulverization, and fading. However, such processes of deterioration in wall paintings are manifested with the participation of water [30]. Under the influence of AP fluctuation, the rise and fall of earth-air can cause frequent exchange between the atmosphere and earth-air, leading to frequent alternation between dry and wet air. There is 'fingerprint' evidence of exchange between AP and the humidity of earth-air [23]. Therefore, earth-air activity can influence the cave environment, and vice versa. For the wall paining interface, this process can lead to repeated crystallization of salts that can cause irreversible damage.

Previously, air humidity has been used as an indicator to reveal the existence of earth-air activity through the relationship between relative humidity and AP [23]. However, earth-air flow is the most direct evidence of rising/falling earth-air activity. For a long time, owing to lack of equipment with which to directly measure earth-air flow, the quantity of the actual earth-air flow in the process of AP fluctuation activity, and the regularity and spatiotemporal distribution of earth-air activity have remained unclear. Therefore, determining how best to quantitatively monitor the quantity and spatial distribution of earth-air activity is crucial in relation to preservation of the wall paintings in the Mogao Grottoes. Scientific monitoring of the quantity and characteristics of earth-air activity of the ground and the four walls of the caves could reveal the spatiotemporal distribution and regularity of earth-air activity in the interior of the cave, which would be of great importance for the protection of the cultural relics.

Recently, our team invented a device for monitoring earth-air flow and used it to preliminarily reveal the quantity, regularity, and formation mechanism of earth-air activity outside the caves of the Mogao Grottoes on yearly and daily scales. This demonstrated the
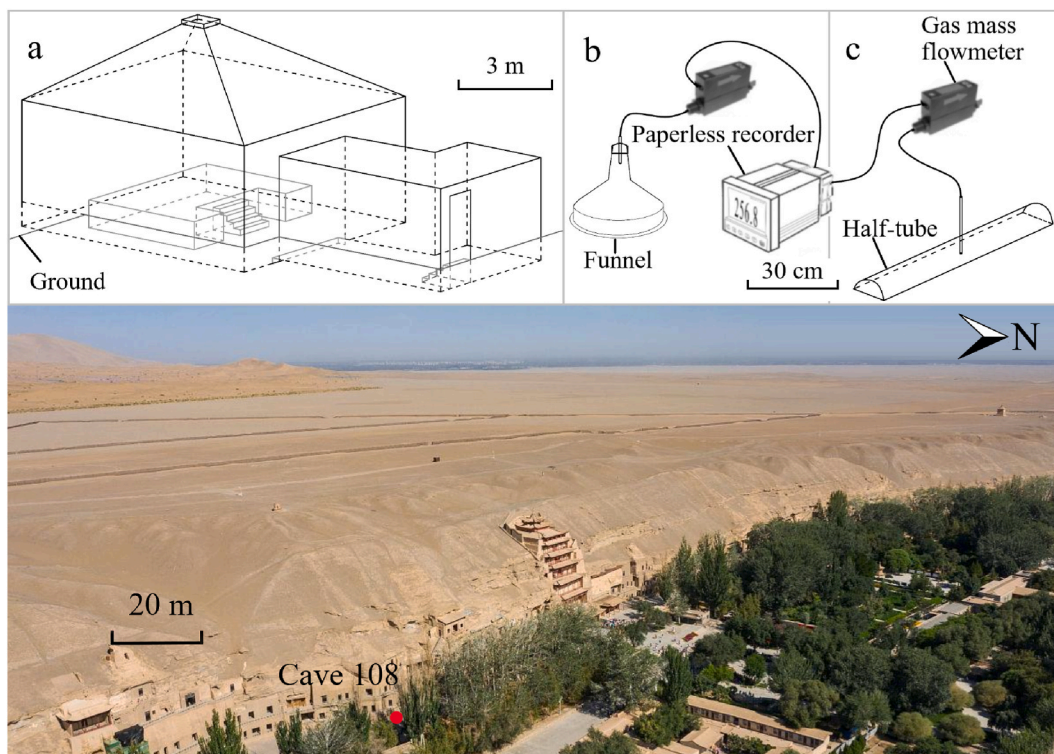
Fig. 1. Schematics of experimental Cave 108 and the monitoring device, and photo of the study area.

applicability of the technical approach and provided a research foundation for the monitoring of earth-air in caves. The importance of earth-air activities in the caves of the Mogao Grottoes was not considered in the past when measures were adopted for the protection of the cultural relics. For example, the floor of some caves has been hardened with concrete, resulting in a certain degree of ground surface closure that might have affected the earth-air activity and endangered the cave wall paintings. Therefore, it is urgent that research be conducted to monitor the earth-air activities and to investigate the related sealing issues in caves.

Based on the above, we installed a large number of earth-air flow monitoring devices in Cave 108, which was selected as a typical representative cave of the Mogao Grottoes. Through comprehensive monitoring, we elucidated the quantity and patterns of earth-air activity and identified the spatiotemporal distribution characteristics and flow patterns of earth-air within the caves. Additionally, we analyzed various influencing factors (such as surrounding rock texture, wall vertical height, and porosity) contributing to spatial variations in earth-air distribution. This analysis provides a scientific basis for understanding the formation mechanism of cave wall painting deterioration. Additionally, our quantitative analysis of earth-air in the studied cave has universal relevance and could provide new insights for related fields of built environment.

2. Materials and methods

2.1. Research area, cave, and monitoring device

The site of the Dunhuang Mogao Grottoes is at the southern edge of the Dunhuang Basin (40°02′14″N, 94°47′38″ E; elevation: 1350 m), which is a typical extremely arid zone in China [31]. The cave group, dug into a 30–50 m high consolidated conglomerate cliff of the Quaternary Jiuquan Formation on the west bank of Daquan River Valley at the junction of Sanwei Mountain and Mingsha Mountain. The cliff consists of cemented gravel sandstone, which has aerated porosity of 20%–30% and dry bulk density of 1.98–2.62 g/m^3 [32]. The conglomerate bedding of sandstone is clear, the composition is mainly metamorphic rock, the particle size is generally 1–3 cm, the maximum is 8 cm, with sorting and directional arrangement [33,34]. Locally, the intensity of solar radiation can reach 1.10 kW/m^2, the annual sunshine rate is 71%, the annual average wind speed is 4.10 m/s, and annual precipitation is 42.20 mm.

We selected Cave 108 in the lower layer as the location for the monitoring in this study (Fig. 1). This cave was excavated in the Five Dynasties period, i.e., approximately 1100 years ago. It is a large cave with an inverted funnel-shaped roof and it is now semi-underground. Quicksand has been deposited in the area outside of the cave, resulting in the floor level of the cave now being 1.41 m below the ground level of the exterior [35]. There are no wall paintings on the surrounding rock in the front room of the cave, and the ground is covered with a layer of quicksand (thickness: ~3 cm). Most of the wall paintings on the west wall of the cave have fallen off, and some of the wall paintings on the north and south walls are missing.

The surrounding rock of the cave comprises alternating layers of thick-bedded fine conglomerate and thin-bedded conglomerate, with particle sizes of 5.20–12.20 mm. The water content of the surface surrounding rock is 0.20%, while that of the deep layer of the
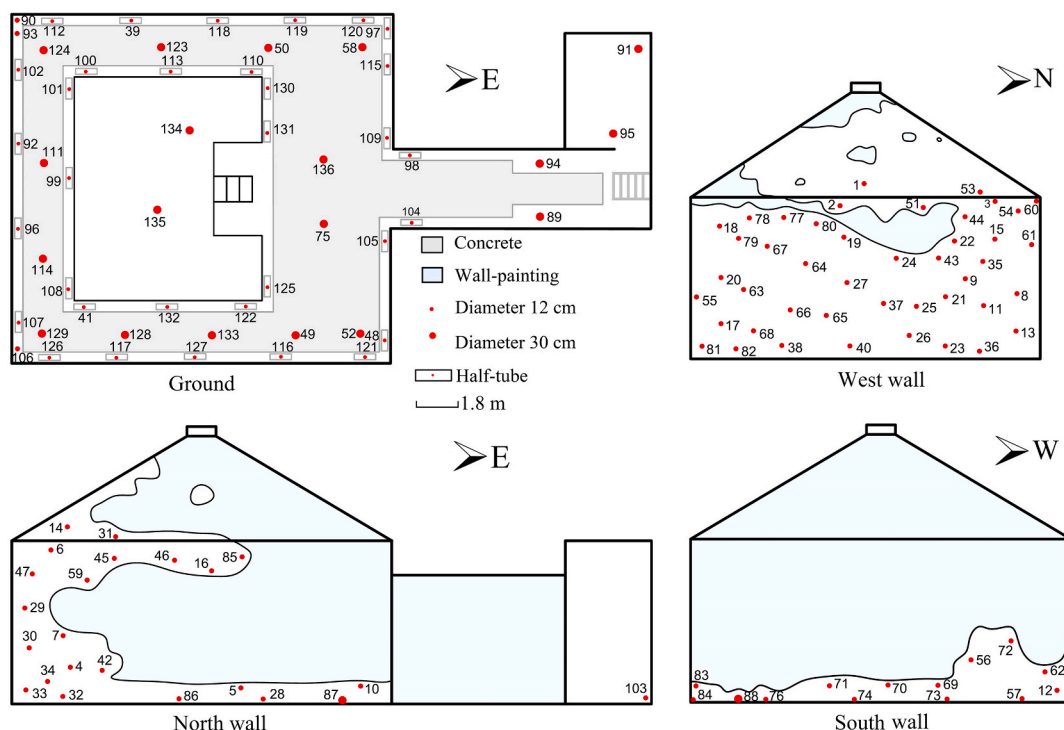
Fig. 2. Schematics of the earth-air monitoring points in Cave 108.

cliff can reach 1.10%. Given the minimal water content in both the plaster layer and surrounding rock are extremely low, there exists, only the combined water, no is present; capillary water is absent [28]. Phreatic water evaporation has been occurring and leaving rich salts (~3.5%) in wall painting and the caves' surrounding rock of 0.5 m in depth [36]. More than 50% of the salt present is mirabilite. The number of water molecules of mirabilite changes from 10 to 0 depending on relative humidity [6]. When relative humidity exceeds 62.5%, the mirabilite in wall paintings becomes deliquescent; when the humidity subsequently drops below 62.5%, the dissolved mirabilite will crystallize again [37].

The cave is composed of three parts: the front room, a corridor, and the main room. The main room is 11.3-m long and 10.4-m wide, with four walls that are 5.0 m high but with a maximum ceiling height of 8.2 m. The corridor is 5.5-m long, 2.8-m wide, and 4.0-m high. The front room is 2.7-m wide, 3.6-m long, and 4.0-m high [38,39]. The total volume of the cave is approximately 842 m^3, and the total surface area is approximately 655 m^2. The cave experiences seasonal temperature variations, but the diurnal temperature fluctuation is minor and can be disregarded (see Fig. S3). The floor of the cave is covered with concrete, leaving an interstice of 10–15 cm near the surrounding walls and the Buddha altar to facilitate the possible release of underground moisture. We conducted earth-air flow monitoring on areas of the surrounding rock without wall paintings and on the ground (see Fig. S2).

Earth-air flow monitoring was conducted using an MF4003 gas mass flowmeter, together with a funnel with a large-end diameter of 12 cm (Fig. 1b) or a half-tube (polyvinyl chloride half-tube with both ends closed) with diameter of 5 cm and length of 50 cm, which was used for monitoring the concrete floor interstices (Fig. 1c). The concrete floor itself was monitored using a funnel with a large-end diameter of 30 cm. Additionally, holes with a diameter of 3 cm and a depth of 30 cm in the west wall, made in a previous experiment (monitoring points No. 1, No. 13, No. 18, and No. 20), were monitored using a small funnel. The MF4003 gas mass flowmeter has a pipe with diameter of 3 mm, a working temperature of −10 to 50 °C, full scale (FS) of 2 L/min, accuracy of ±(1.50 + 0.20 FS)%, display resolution of 0.001, and response time of 10 ms. Prior to experimental monitoring, we meticulously calibrated all gas mass flowmeters in series. The AP in Cave 108 was monitored using a barometric transmitter (model HD9408TBARO, made in Italy) accurate to ± 0.5 hPa at 20 °C. At point No. 20, a thermohygrometer (Onset, HOBO-U23-001, made in the USA), accurate to ± 0.2 °C in the range 0–50 °C and to ± 4% (±2.50%) in the relative humidity range of 0%–10% (10%–90%), was used to monitor temperature, humidity, and the inflow of earth-air, and the resulting data were used to calculate the absolute humidity, and to analyze the relationship between earth-air activity and absolute humidity. The monitoring interval of all sensors was 10 min. Overall, 136 monitoring points were established in Cave 108 (Fig. 2).

2.2. Model and research method of earth-air activity

We regard the underground saturated belt as a closed bottom layer, and the ground from the surface to the saturated belt, i.e., the vadose zone, as a closed space covered by the external atmosphere. We can consider earth-air as an ideal gas [22,23]. Therefore, in the process of AP activity, considering the entire vadose zone as a closed space, we can use Boyle's law ($P_1 V_1 = P_2 V_2$) to calculate the variable quantity of earth-air as follows:

$$\Delta V = \frac{(P_1 - P_2) \times n \times t}{P_2} \tag{1}$$

where ΔV refers to the amount of earth-air activity ($\Delta V = V_1 - V_2$, where V_1 and V_2 refer to the volume when the external AP changes from P_1 to P_2, respectively), n is the aerated porosity, and t is the thickness of the vadose zone. When $P_1 - P_2 > 0$, it means that AP has decreased and that earth-air has risen upwards, allowing moist earth-air to flow out. Conversely, when $P_1 - P_2 < 0$, it means that AP has increased and earth-air has retreated downwards, allowing dry air to enter. The rise and fall of earth-air can cause alternation in dry and wet air at the wall painting interface. The fluctuation of AP is the main factor driving change in the quantity of earth-air activity. The quantity of earth-air activity is positively correlated with the amplitude and frequency of AP fluctuation, the thickness of the vadose zone, and the aerated porosity.

To fully understand the spatial distribution of earth-air outflow in Cave 108, it was necessary to establish a large number of monitoring points. We considered multiple batches of distribution points on the surrounding rock and ground of Cave 108. According to Eq. (1), the fluctuation range of $|P_1 - P_2|$ is the main factor affecting the magnitude of earth-air flow, and the two aspects are directly proportional. However, during different periods, the same monitoring point exhibits seasonal variations. Based on the ideal gas equation, $V = nRT/P$, when the temperature is higher, the amount of water and other gases released by the soil (n) increases. Furthermore, the AP is lower in the summer. When experiencing the same fluctuation in AP, the earth-air flow is higher in summer, and conversely in winter. Hence, there are distinct differences in earth-air flow when subjected to the same AP fluctuation. Factors such as temperature, seasonal pressure, AP fluctuation, and soil earth-air hysteresis exert significant effects on the earth-air flow. Therefore, if we monitored earth-air outflow in batches, we could determine the earth-air outflow at different points at the same time, but we could not establish and compare the earth-air outflow at different points at different times. For this purpose, we selected four drilling holes and monitoring point No. 3 (without a hole) on the west wall for annual monitoring and used the other monitoring points for monitoring over a period of approximately 1 month. Among them, point No. 1 on the west roof was selected as the reference object for different points in other different periods. The annual flow monitored at point No. 1 was used to determine the annual relative earth-air outflow at other monitoring points using the following formula:

$$\frac{\overline{F_{pt}}}{\Delta |P_1 - P_2|_t} \bigg/ \frac{\overline{F_p}}{\Delta |P_1 - P_2|} = \frac{\overline{F_{1t}}}{\Delta |P_1 - P_2|_t} \bigg/ \frac{\overline{F_1}}{\Delta |P_1 - P_2|} \tag{2}$$

where $\overline{F_p}$ is the annual average relative earth-air outflow at a point, $\overline{F_{pt}}$ refers to the average value of earth-air outflow at the point during time t, $\overline{F_1}$ refers to the average annual earth-air outflow at point No. 1, $\overline{F_{1t}}$ refers to the average earth-air outflow during period t at point No. 1, $\Delta\overline{|P_1 - P_2|}_t$ refers to the average value of the absolute amplitude of AP fluctuation during time t, $\Delta\overline{|P_1 - P_2|}$ refers to the average value of the absolute amplitude of AP fluctuation throughout the year, and P_2 is the AP at which earth-air enters and exits equilibrium (i.e., the earth-air outflow is 0), which varies with the annual AP trend (Fig. 3a).

Thus, the annual relative earth-air outflow $\overline{F_p}$ at a monitoring point can be determined as follows:

$$\overline{F_p} = \frac{\overline{F_{pt}} \times \overline{F_1}}{\overline{F_{1t}}} \tag{3}$$

and the per unit area earth-air outflow F_p at a monitoring point can be calculated as follows:

$$F_p = \overline{F_p}/S \tag{4}$$
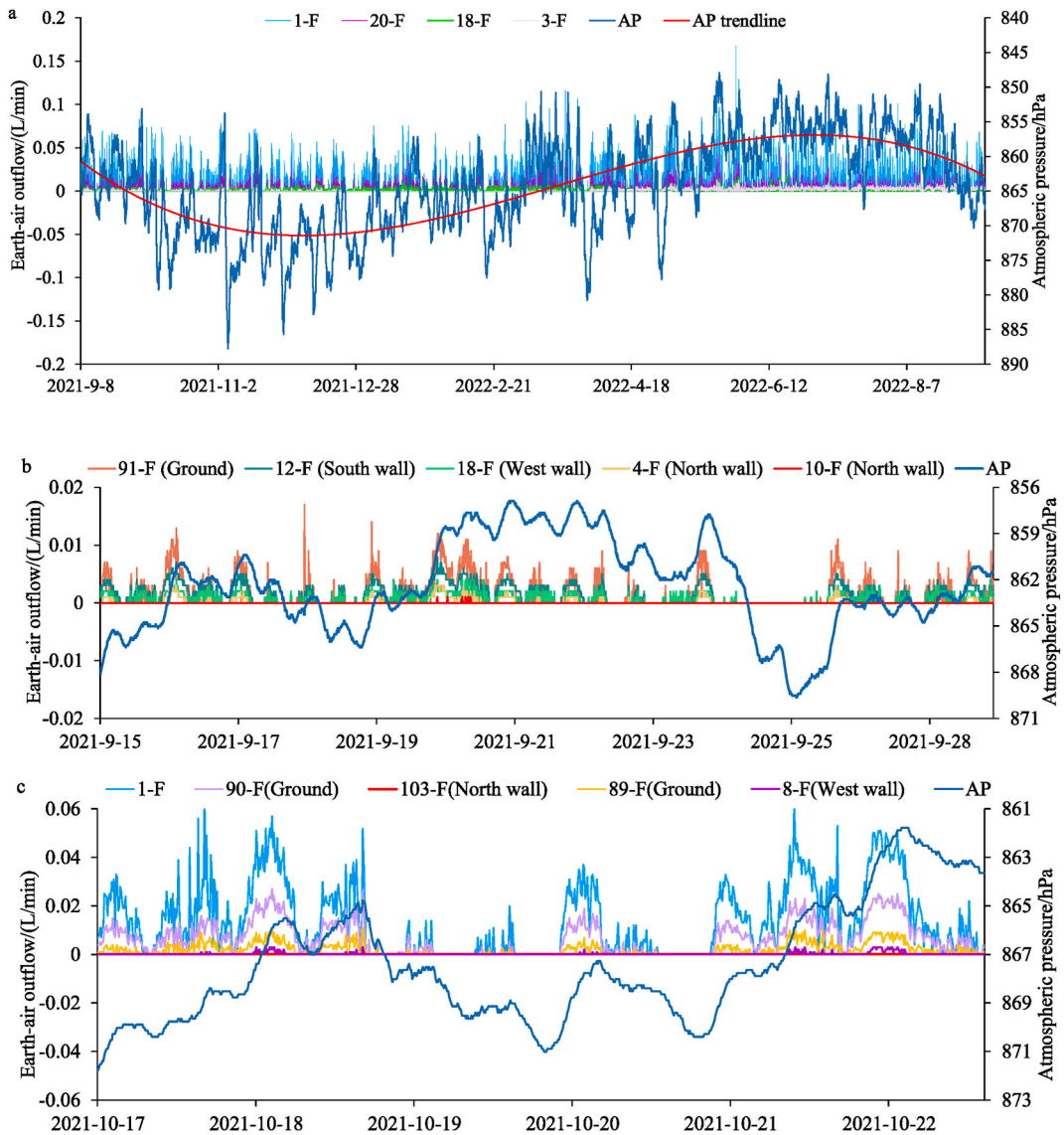
Fig. 3. Variation characteristics of earth-air outflow/flux, AP, relative humidity, and absolute humidity at the monitoring points in Cave 108. (a) annual variation of monitoring points and AP in the west wall; (b) changes of earth-air outflow from ground, west wall, south wall, north wall and AP in September; (c) changes of earth-air outflow from ground, west wall, north wall and AP in October; (d) changes of earth-air outflow from ground, west wall and AP in May; (e) earth-air flux (include earth-air outflow and inflow) and relative humidity, absolute humidity and AP. Orange box areas in panel a correspond to the periods shown in panels b–e).
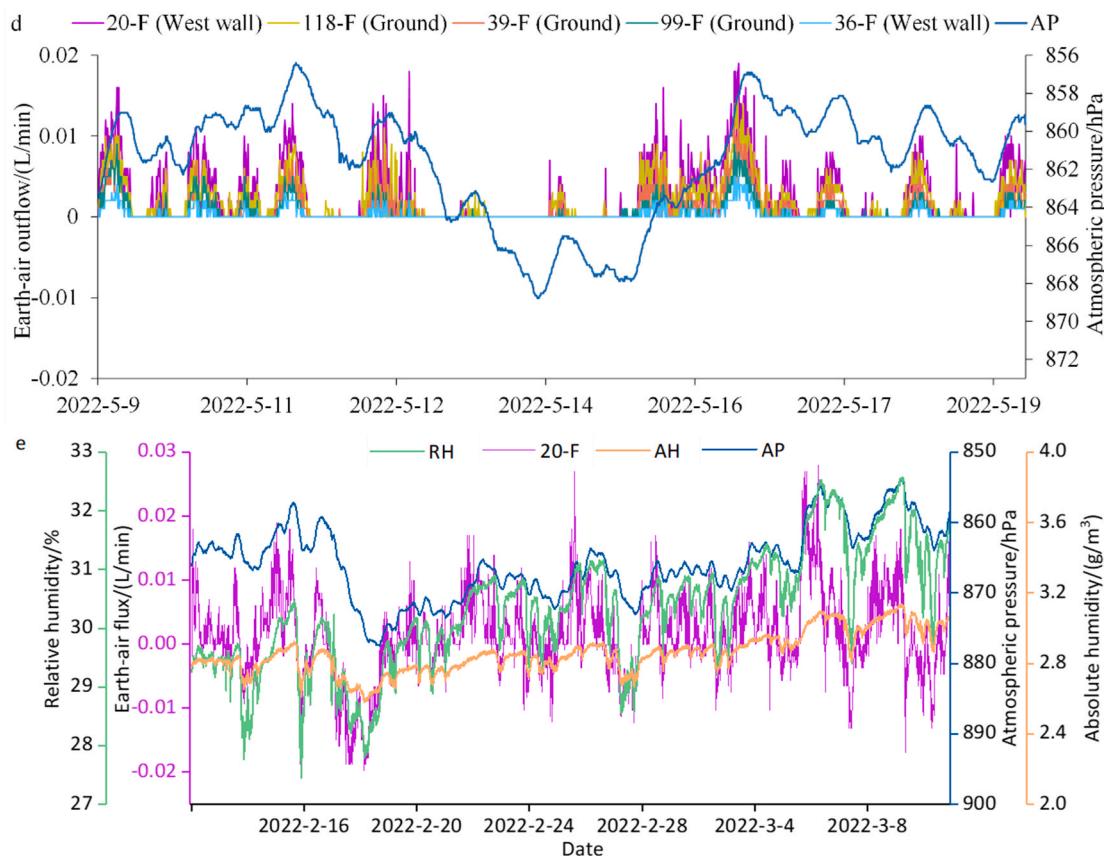
Fig. 3. (*continued*).

where S is the area of the monitoring equipment. For example, the area of the funnel with diameter of 12 cm is 113 cm^2, and the area of the half-tube is 250 cm^2. Then, the spatial distribution of earth-air outflow in the cave was mapped based on F_p. The spatial distributions of the ground and walls were mapped using the inverse distance weight (IDW) method in ArcGIS 10.5.

This study determined the quantity and characteristics of earth-air activity, and defined the spatiotemporal distribution of earth-air outflow through quantitative and batch monitoring of earth-air outflow on the Cave 108. Using a closed system model, combined with consideration of the geological structure and pore size at the monitoring points, the reasons for the spatial differences in earth-air outflow were analyzed. Moreover, the effects of concrete flooring, wall orientation, and vertical height on efflorescence in the cave were investigated.

3. Results and analysis

3.1. Variation characteristics of earth-air flow in the cave

Based on data acquired during more than one year of continuous monitoring, Fig. 3 shows the change in earth-air outflow at representative monitoring points on the ground and surrounding rock in Cave 108. The variation in earth-air outflow is closely related to fluctuation in AP. The earth-air outflow at fixed monitoring points fluctuated synchronously but with clear differences in magnitude (Fig. 3a). The earth-air annual outflow at Nos. 1, 3, 13, 18, and 20 was 5704, 571, 414, 584, and 1660 L, respectively. Temperature is another important factor that can affect the earth-air outflow (see Fig. S3). Seasonal differences were found with earth-air outflow in summer obviously greater than that in winter. Conversely, AP was lower in summer than in winter, with a range of fluctuation of approximately 10–30 hPa. The vertical coordinate of AP in Fig. 3 is the reverse scale value, which means that the two variables fluctuated synchronously in opposite directions, i.e., as AP increased, earth-air outflow decreased; as AP dropped, earth-air outflow increased, leading to moist earth-air outflow (see Table S1). This confirmed that the earth-air closed model (i.e., Eq. (1)) is correct, and that AP is the dominant cause of earth-air activity.

To better analyze the synchronicities and disparities in earth-air outflows at monitoring points within Cave 108, we have selected monitoring batches encompassing both ground and wall points for our observational period. At different times, earth-air outflow at the monitoring points of the three walls and ground of the main room and at the fixed monitoring points (Nos. 1, 18, and 20) in Cave 108

fluctuated synchronously with the change in AP (Fig. 3b–d). However, there were differences in the magnitude of earth-air activity at different monitoring points at the same time. In addition to AP fluctuations that can affect earth-air outflow, the geological structure at the monitoring points can also have certain impact on the degree of earth-air activity, resulting in uneven flow distribution. The outflow of earth-air at point No. 91 was 1.36, 2.02, 3.68, and 5.46 times greater than that at No. 12 (south wall), No. 18 (west wall), No. 4 (north wall), and No. 10 (north wall), respectively (Fig. 3b). The outflow at No. 10 represents a typical pulse-like earth-air fluctuation (Fig. 3b). Only at times of marked change in the weather does this type of earth-air outflow occasionally show a pulse; at all other times, it is static. In Fig. 3c, the earth-air outflow at point No. 1 was 2.05, 5.22, and 15.44 times larger than that at No. 90 (ground), No. 89 (ground), and No. 8 (west wall), respectively. There were also monitoring points where the outflow of earth-air showed no response to AP and was always zero (e.g., No. 103). In Fig. 3d, the outflow at point No. 20 on the west wall was 1.10, 1.90, 2.24, and 4.31 times greater than that at No. 118 (ground), No. 39 (ground), No. 99 (ground), and No. 36 (west wall), respectively. All monitoring results showed that the flow of earth-air fluctuated synchronously.

We also monitored the quantity of earth-air flow into the soil in the hole at point No. 20 (Fig. 3e). The outflow of earth-air was positive while the inflow was negative. Therefore, in the discontinuity period of outflow shown in Fig. 3a–d, there is still earth-air inflow. Earth-air flux is inversely proportional to AP and proportional to relative humidity and absolute humidity. If equilibrium exists between the internal and external pressures of the soil before AP fluctuates, when the AP drops, earth-air rises, moist earth-air flows out of the surface, the relative humidity rises, and the water vapor concentration in the air increases, the moist earth-air causes salt to dissolve. Conversely, when the AP rises, earth-air falls, dry air enters the surface, the relative humidity decreases, and the water vapor concentration in the air decreases, the crystallization of salt is pulverized. This shows that the rise and fall process of earth-air will cause alternation of dry and wet air. However, on the wall painting interface, alternation of dry and wet air will lead to repeated crystallization of salt, thereby changing the structure of the surface, and resulting in salt-related deterioration and irreversible damage to the cave wall paintings.

3.2. Spatial distribution characteristics of earth-air outflow in the cave

To comprehensively understand the spatial distribution characteristics of earth-air outflow in Cave 108, we considered the earth-air outflow at 136 monitoring points on the ground and surrounding rock as basic data, calculated the per unit area of earth-air outflow (F_p) at each point (see Table S2).

3.2.1. Spatial distribution of earth-air outflow in Cave 108

The spatial distribution of earth-air outflow on the ground is shown in Fig. 4.

According to the values of ground F_p calculated using Eq. (3), the average ground earth-air outflow of the 55 points was 0.109 L/(min·m²) (Fig. 4). From the perspective of the spatial distribution pattern, the greatest earth-air outflow was at the interstices between the concrete floor and the surrounding walls of Cave 108. Comparison of the outflow of earth-air from the interstices of the surrounding walls revealed that the outflow of earth-air at the interstice of the east wall was smallest, with an average value of 0.017 L/(min·m²). The outflow at the interstice beside the west wall was the largest, with an average value of 0.705 L/(min·m²), i.e., 41.47 times that of the interstice beside the east wall. The mean value of earth-air outflow at the interstice beside the south wall and the north
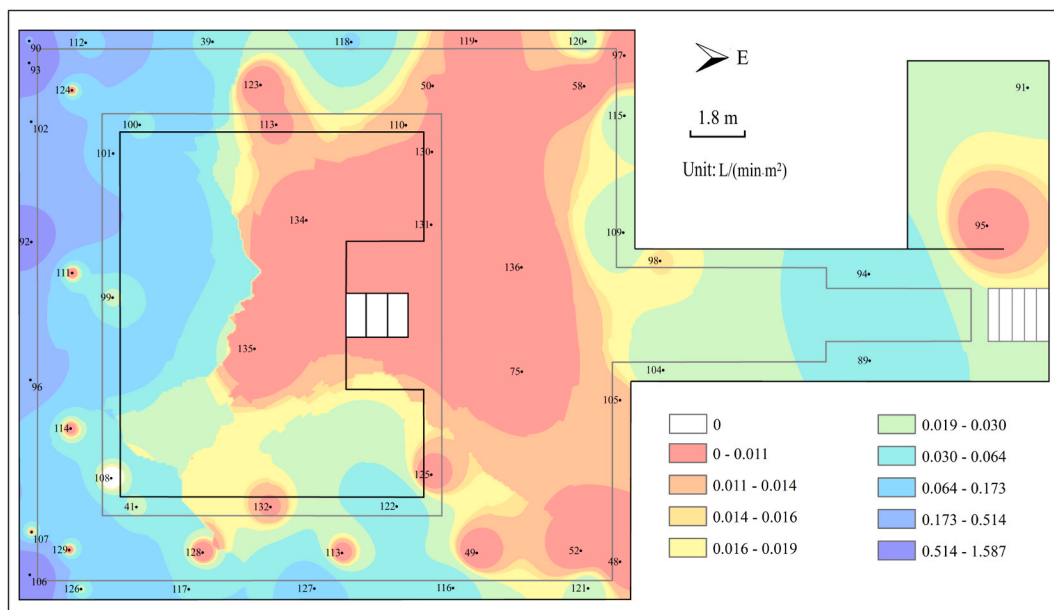
Fig. 4. Spatial distribution of earth-air outflow on the ground in Cave 108.

wall was 0.056 and 0.047 L/(min·m^2), respectively. The earth-air outflow on the west side was larger than that on the east side of the north wall interstices, showing a trend of reduction from the west to the east. The spatial distribution pattern of earth-air outflow at the interstices around the Buddha altar was consistent with that at the interstices of the surrounding walls, i.e., that on the west side was largest (average value: 0.035 L/(min·m^2)), followed by that on the south and north sides (average value: 0.028 and 0.020 L/(min·m^2), respectively), while that on the east side was smallest (average value: 0.002 L/(min·m^2)). The average earth-air outflow from the concrete floor of the cave was 0.003 L/(min·m^2), that from the quicksand-covered area of the front room was 0.013 L/(min·m^2), and that of ground without cover was 0.046 L/(min·m^2), i.e., the earth-air outflow of uncovered ground and quicksand-covered ground was 15.33 and 4.33 times greater than that of the concrete floor, respectively.

3.2.2. Spatial distribution of earth-air outflow on the west wall

The spatial distribution of the outflow of earth-air on the west wall and the west roof of Cave 108 is shown in Fig. 5. It is worth noting that, for security reasons, we established only two monitoring points on the west roof of the cave. In Fig. 5, the white area on the west wall indicates an unresponsive area (i.e., earth-air outflow of zero).

The average and maximum outflow of earth-air on the west wall was 0.041 and 0.285 L/(min·m^2), respectively. It is evident from Fig. 5 that the vertical distribution of earth-air outflow was inversely proportional to height, i.e., the greater the height, the smaller the magnitude of earth-air outflow. Overall, the outflow of earth-air from the south side of the west wall was greater than that from the north side. However, the earth-air outflow at point No. 61 was much greater than that of the surrounding area, reaching 0.285 L/(min·m^2). This might be related to the relatively loose rock structure at this point. We also found areas on the west wall where there was no earth-air activity (e.g., Nos. 15, 22, 26, 35, and 77, these data are shown in data S1 and Fig. S4). This might be related to the dense rock structure and the poor permeability in those areas (see Fig. S2). It should be noted that the outflow of earth-air from the remaining drill holes (i.e., Nos. 17, 20, and 18) in the west wall was much greater than that in surrounding areas, and that the drill hole structure had a certain effect of accumulation on earth-air. Using point No. 20 as reference, earth-air outflow was found to be seven times larger than that at the surrounding points. Therefore, the values at the three drill holes were reduced by a factor of seven to determine the actual earth-air outflow at those points on the west wall.

3.2.3. Spatial distribution of earth-air outflow on the north wall

The spatial distribution of earth-air outflow on the north wall and the north roof is shown in Fig. 6. The average value was 0.035 L/(min·m^2). As in Fig. 6, the white area on the north wall of the cave shown in Fig. 6 indicates an unresponsive area.

The outflow of earth-air decreased with increasing height, but with some differences between the west wall and the north wall at different heights and different points (Figs. 5 and 6). The maximum outflow of earth-air on the north wall was 0.36 L/(min·m^2), i.e., 1.28 times greater than that on the west wall (Table S2). Additionally, the outflow of earth-air on the north wall showed a trend of reduction from the west to the east. With consideration of Fig. 4, it is evident that the spatial distribution of the outflow of earth-air in the cave showed a notable characteristic of reduction from the inside to the outside. The cliff has important influence on the quantity of
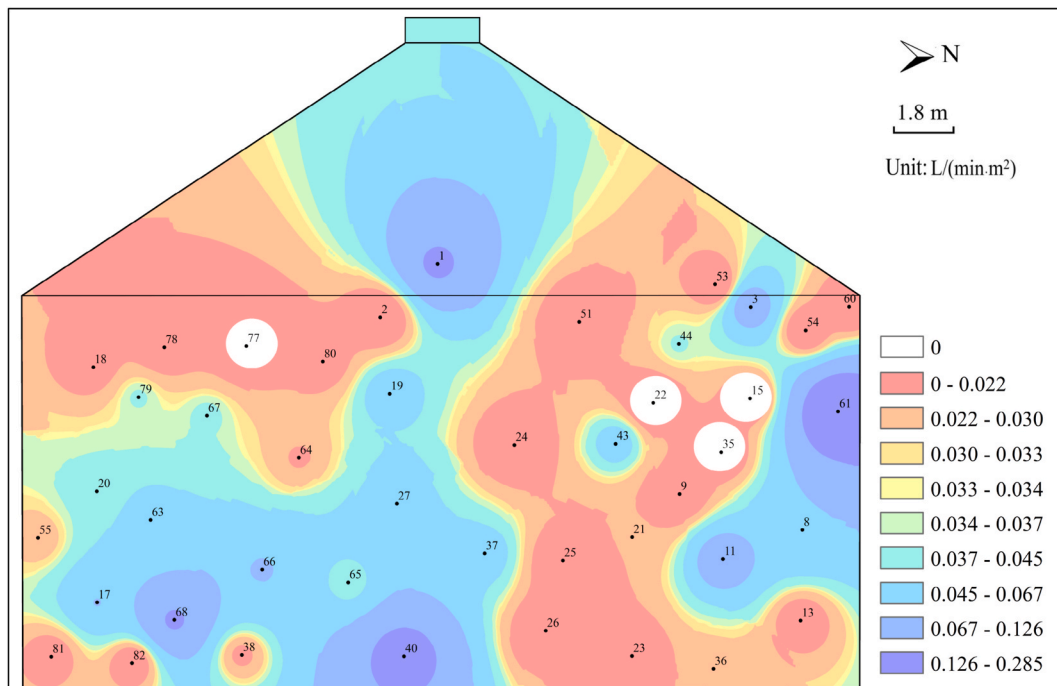
Fig. 5. Spatial distribution of earth-air outflow on the west wall and the west roof of Cave 108.
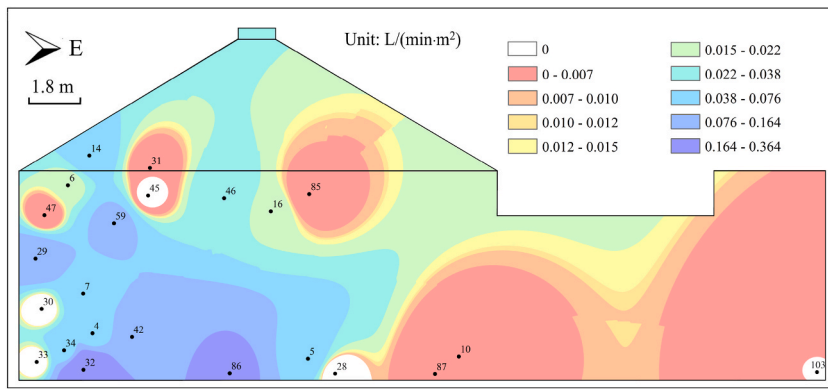
Fig. 6. Spatial distribution of earth-air outflow on the north wall and the north roof of Cave 108.

earth-air outflow, and the deeper the position within the cliff, the greater the amount of earth-air outflow.

3.2.4. Spatial distribution of earth-air outflow on the south wall

The spatial distribution of earth-air outflow from the south wall of Cave 108 is shown in Fig. 7. The average and maximum value of the outflow of earth-air from the south wall was 0.081 and 0.599 L/(min·m^2), respectively. Owing to the intact preservation of the wall paintings higher up on the south wall, the monitoring points were placed lower down. With consideration of Figs. 5 and 6, it is evident that the wall painting plaster layer caused the average value of earth-air outflow on the south wall to be larger. The results of the monitoring on the lower part of the south wall could not completely represent the earth-air outflow of the entire south wall. As shown in Fig. 7, the outflow of earth-air from the surrounding rock near the ground on the south wall reduced from the bottom to the top, indicating that earth-air outflow in the surrounding rock higher above the ground was less active and had less influence on the wall paintings. This also shows that strong earth-air activity is the main reason for the formation of near-ground efflorescence belts in the caves.

3.2.5. Summary of earth-air outflow in Cave 108

The results of the classification revealed obvious similarities but also some differences in the spatial distribution of earth-air outflow in the surrounding rock and ground of Cave 108. On the ground, higher earth-air outflow was mainly concentrated on the west wall interstice, while the highest earth-air outflow on each of the three walls of the cave was concentrated in the lower layer of the
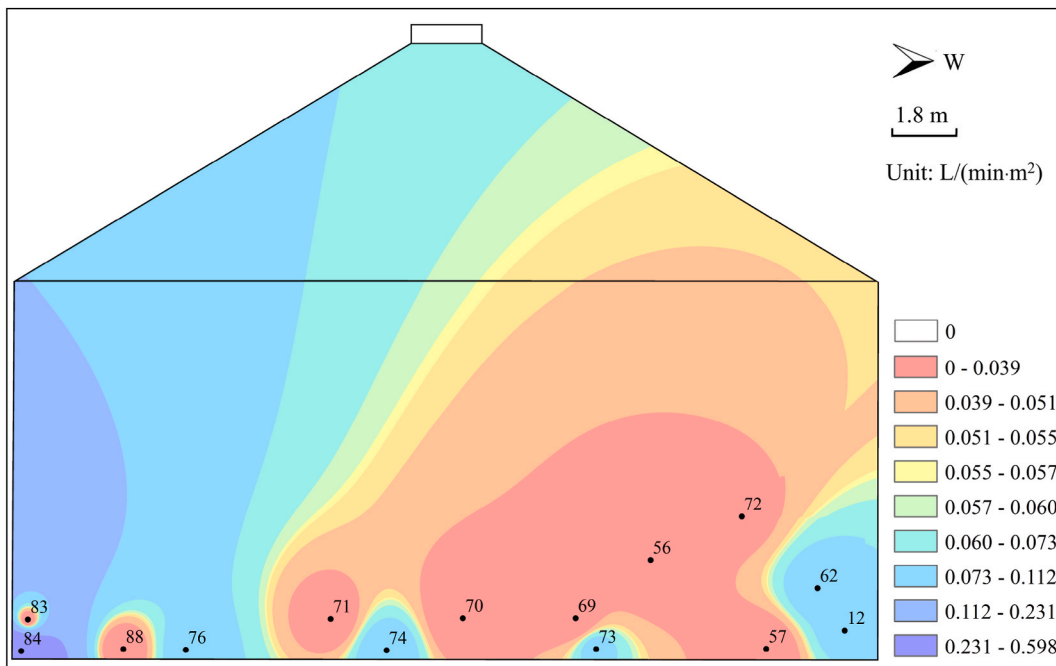
Fig. 7. Spatial distribution of earth-air outflow on the south wall of Cave 108.

surrounding rock. It should be noted that the clay-textured plaster layer will weaken the earth-air flow, resulting in a smaller earth-air outflow in the wall paintings covered area.

The spatial distribution of earth-air outflow from around the walls of the cave was extremely uneven, with marked differences. However, those points with earth-air outflow of >0.120 L/(min·m²) were all concentrated in the lower layer of the surrounding rock and at the interstice of the west wall and ground, which reflects that the spatial distribution of earth-air outflow of each of the four walls of the cave had certain similarity and regularity. It also shows that the formation of the efflorescence belt in the cave is closely related to this characteristic.

It should be noted that point No. 84 (Fig. 7) is unique, and that the rock layer at that location might be a natural channel for earth-air release, which resulted in a value of earth-air outflow of up to 0.599 L/(min·m²). Excluding point No. 84, the average outflow of earth-air on the south wall was 0.041 L/(min·m²). However, because the monitoring points on the south wall were mainly concentrated in the lower part, the average earth-air outflow on the south wall was larger than that of the other walls. For this reason, we averaged the outflow of earth-air at the monitoring points below the equivalent height (i.e., 2.0 m) on both the west wall and the north wall, which produced a value of 0.062 and 0.053 L/(min·m²), respectively. Therefore, the overall spatial distribution of earth-air outflow in Cave 108 showed the following pattern: ground > west wall > north wall > south wall.

4. Discussion

4.1. Effect of AP equilibrium point on earth-air outflow

According to the closed system model, i.e., Eq. (1), $\Delta V = \frac{(P_1 - P_2) \times n \times t}{P_2}$, and the fluctuation of $|P_1 - P_2|$ is proportional to the flow, which means that the value of P_2 can directly affect the magnitude of F_p. Adopting the annual average value of P_2 in Eq. (1) would lead to a larger value of $|P_1 - P_2|$ in the calculation results. Thus, choosing the inflow and outflow equilibrium point of earth-air, i.e., when the earth-air outflow is zero for the AP of P_2, makes the result of the $|P_1 - P_2|$ calculation more accurate. In the calculation process adopted in this study, the value of P_2 was determined according to the earth-air outflow at reference point No. 1 and the AP change process. Overall, a value of P_2 was calculated 56 times during the year, and its distribution curve was found broadly consistent with the AP trend line (Fig. 3a). This allowed more accurate calculation of F_p.

Obviously, in addition to the value of the AP equilibrium point will affect the size of the F_p value, seasonal changes will also exert an influence on the F_p value. For instance, the Mogao Grottoes is windy in spring and autumn, and this weather change process will result in a large change range of AP, which will lead to an increase in the change range of earth-air flow. It is observable from Fig. 3a that the earth-air flow is higher in summer and lower in winter. Moreover, the temperature is difference between the inside and outside of the soil. In winter, when the external cold air flows into the soil it will expand leading to a reduction in the inflow of earth-air. Summer is the opposite. Additionally, seasonal temperature causes water and other gases released/absorbed. This results in the earth-air flow being higher in summer and lower in winter. Amidst the context of AP change, earth-air activity is a prevalent natural occurrence that causes significant damage to cave cultural artifacts. The rise and fall of earth-air activity plays a crucial role in the formation of efflorescent deterioration belts near the ground.

4.2. Influence of closed ground on earth-air outflow

The ground of the main room and the corridor of Cave 108 is laid with poorly permeable concrete. Consequently, the earth-air outflow of the concrete floor was 0.07 and 0.23 times of that of ground without cover and with quicksand cover, respectively. This shows that the concrete floor of the cave has important impact on earth-air activity. The closure reduces earth-air outflow in some areas, but increases earth-air outflow in other areas, especially through the wall paintings, which has adverse impact on their preservation. This finding is consistent with our previous research on the effect of covering boreholes with different types and thicknesses of soil on passive respiration [23]. It is evident from Fig. 4 that the outflow of earth-air at the interstices of the four walls and the interstice of the Buddha altar was substantially greater than that of the concrete floor. This further confirms that the laying of concrete or quicksand on the floor of the cave will have consequential impact on the earth-air outflow of the ground, causing lateral flow of earth-air that promotes increase in earth-air outflow at the interstices of the four walls and from the four walls.

Therefore, laying a concrete floor in the caves is not conducive to the outflow of earth-air and to the protection of the wall paintings, and such floor covering should be removed. Moreover, increasing earth-air flow in areas of the wall without paintings would be beneficial to reducing the flow in areas of the wall painting interface.

4.3. Influence of geological background on earth-air outflow

The monitoring results of a group of monitoring points (Nos. 18, 20, and 17) arranged vertically on the west wall from high to low (Fig. 5) showed that earth-air outflow occurred over the entire vertical surface of the west wall, but that the outflow of earth-air decreased with height. This is because the caves penetrate deep into the cliff and lie in the vadose zone with a background of ~200 m; therefore, earth-air activity varies at different heights throughout the caves. For freestanding wall based models, when earth-air rises to a certain height, it will disappear, and only near-ground efflorescence belts will be formed [28]. In other words, owing to the existence of the cliff and the cave structure, earth-air flow through the Gobi Desert from the top of the cave has formed a 'shortcut' that increases the earth-air flow to a certain extent. Thus, the entire cave walls/cliff structure has earth-air flow but with a higher level of

activity in the lower layer. This is also proved by the high earth-air flow in the surrounding rock near the ground. Because the west wall of the cave is set deepest into the cliff, strong earth-air outflow has particularly serious impact on the west wall, which has resulted in almost all the wall paintings falling off (Fig. 5). This phenomenon is not specific to Cave 108. In many caves, the paintings on the west wall have fallen off or are seriously deteriorated, and the degree of deterioration is obviously higher than that of the paintings on other walls.

According to Figs. 5–7, the average outflow of earth-air on the west wall was 0.021 and 0.009 L/(min·m^2) larger than that on the north and south walls, respectively. In comparison with the south wall, the north wall of the cave is affected more by the cliff. The north wall is completely embedded within the cliff, while only 20% on the west side of the south wall is completely embedded within the cliff; the remainder of the south wall is at the turning point of the cliff with thin surrounding rock (Fig. 1), which reduces both the quantity of earth-air activity and the influence of alternation of dry and wet air to some extent. Therefore, the wall paintings on the south wall of the cave are reasonably well preserved, except for the lower part.

The spatial distribution of earth-air outflow on the west wall is similar to that on the north wall, but with some differences in the earth-air outflow in different areas. This is mainly caused by differences in the local texture of the surrounding rock. The surrounding rock of the Mogao Grottoes is Jiuquan sand conglomerate with large pores [40]. The characteristics of the horizontal diluvial layer in the rock surrounding the cave are obvious, and the composition of the material is mixed, with irregular bedding and interlayering that lead to uneven pores and obvious differences in the surrounding rock. The coarser the particles of the diluvial layer, and the more favorable the permeability of the structure for earth-air activity (such as at point No. 1). Alternating movement of dry and wet air through the wall paintings will inevitably lead to repeated crystallization of salt and ultimately cause deterioration of the wall paintings. The dense and well-cemented surrounding rock has poor permeability, and there is almost no flow in this area, which is very conducive to the preservation of wall paintings. Therefore, the addition of special exhaust holes in the cave would be conducive to the protection of the wall paintings.

4.4. Evaluation of total quantity of earth-air and its effects

The total area of Cave 108 is approximately 655 m^2. With consideration of the average quantity of earth-air outflow from the ground and the four walls of the cave (see Table S3), we estimated the earth-air outflow from the cave to be approximately 50.89 m^3/d. Although we have not monitored the earth-air inflow in Cave 108, according to the principle of balance between earth-air inflow and outflow, the daily earth-air inflow into Cave 108 should be 50.89 m^3/d. Under the influence of the daily fluctuation of AP, there is frequent exchange of dry and wet air between the atmosphere and the earth-air in Cave 108, and the total quantity of air exchange exceeds 101.79 m^3/d.

The cave wall paintings in Cave 108 suffer from serious efflorescence damage, and the near-ground efflorescence is the most serious, even when the surrounding rock is exposed. As is well known, efflorescence is mainly formed with the participation of water. Owing to the action of alternating dry and wet air, salt at the wall painting interface crystallizes repeatedly, thereby changing the structure of the plaster layer and the wall paintings and resulting in efflorescence and salt-related deterioration of the wall paintings [26]. The monitoring results of the near-ground surrounding rocks of the south and north walls showed that greater outflow of earth-air occurred closer to the ground, and that the height of greatest activity was only 20–40 cm above the ground, consistent with the height of observed efflorescence belts. However, it is lower than the theoretical height of 28–112 cm calculated previously [28].

As one of the most important cultural heritage sites in the world, the Dunhuang Mogao Grottoes have entered a stage of proactive preventative protection from a stage of rescue protection. Therefore, we should scientifically deal with the problem of concrete closed ground according to the spatiotemporal distribution and law of earth-air activity, and special earth-air discharge channels should be established to prevent further deterioration of the wall paintings. Additionally, we should also pay attention to the effect of concrete ground hardener, applied in front the caves several years ago, to reduce or eliminate the quantity of lateral flow of earth-air caused by such ground closure, which would also effectively avoid the occurrence of wall painting diseases.

4.5. Limitations and future work

Future research should further enhance the accuracy of earth-air flow monitoring equipment, further synthesize the environmental impact factors of earth-air flow, and enhance the precision of monitoring data for earth-air flow. At this time, this study is limited to a single grotto, which is situated in a unique geographical location and thus may not be representative of the other grottoes in Mogao Grottoes. Future research should take into account the comparison of the spatial distribution of earth-air flow in the upper, middle, and lower caves of Mogao Grottoes.

The behavior of earth-air is influenced by external factors such as temperature, wind speed, wind direction, terrain, and landform, among others. Eq. (2) accounts for some external environmental influences in cave environments. However, Eq. (1) reveals that earth-air activity is also impacted by factors including vadose zone thickness, porosity, bore diameter, cracks, soil structure, composition, soil retardation, earth-air viscosity, and more. As a result, earth-air flow is intricately linked to both external surroundings and internal conditions, forming a complex relationship. The exploration of earth-air represents a novel and challenging realm within the field of built environment research. Investigating influencing factors and the composition of earth-air components (e.g., CO_2, H_2O, H_2, NO_2, CH_4, ^{222}Rn, SO_2, etc.) constitutes a primary focus for our future research endeavors.

5. Conclusions

Using earth-air flow monitoring devices, this study investigated the quantity of earth-air activity at 136 points on the west wall, north wall, south wall, and ground of Cave 108 in the Dunhuang Mogao Grottoes, and analyzed the spatial distribution characteristics of earth-air outflow to reveal the key impact factors. The variation in earth-air outflow was found closely related to AP fluctuation, i.e., it was directly proportional to the outflow of earth-air at the monitoring point and inversely proportional to AP fluctuation. The outflow of earth-air at the interstices of the surrounding walls and ground was found greater than that of the concreted floor, and the outflow of earth-air at the interstice of the west wall was much (41 times) greater than that of the east wall. The outflow of earth-air on the south side of the west wall of the cave was greater than that on the north side. The outflow of earth-air on the north wall near the ground showed a trend of reduction from the west to the east, contrary to that on the south wall, while the outflow in the upper area was generally small. The overall spatial distribution of earth-air activity in Cave 108 showed the following pattern: ground > west wall > north wall > south wall. The earth-air flow of the cave gradually reduced from deep to shallow, from inside to outside, and from high to low. In this study, the air exchange quantity and spatial distribution pattern of earth-air activity in Cave 108 were clarified. It provides a new perspective for mechanism responsible for the damage in wall painting, and plays an important demonstration role in monitoring the earth-air flow in cave-type relics around the world.

Data availability statement

Data will be made available on request. Data to this article can be found online (https://doi.org/10.5281/zenodo.8092824).

CRediT authorship contribution statement

Fei Li: Writing – original draft, Software, Data curation. **Hongshou Li:** Writing – review & editing, Project administration, Funding acquisition. **Shunren Wang:** Supervision, Investigation.

Declaration of competing interest

The authors declare that they have no known competing financial interests or personal relationships that could have appeared to influence the work reported in this paper.

Appendix A. Supplementary data

Supplementary data to this article can be found online at https://doi.org/10.1016/j.heliyon.2024.e25815.

References

[1] B. Panda, S. Chidambaram, Influence of the vadose zone on groundwater pollution—a review, Int. J. Civ. Environ. Agric. Eng. 1 (2019) 41–44, https://doi.org/10.34256/ijceae1916.
[2] G.J. Bouyoucos, M. McCool, The aeration of soils as influenced by air-barometric pressure changes, Soil Sci. 18 (1924) 53–64, https://doi.org/10.1097/00010694-192407000-00004.
[3] X. Kuang, J.J. Jiao, H. Li, Review on airflow in unsaturated zones induced by natural forcings, Water Resour. Res. 49 (2013) 6137–6165, https://doi.org/10.1002/wrcr.20416.
[4] R. Nilson, E. Peterson, K. Lie, N. Burkhard, J. Hearst, Atmospheric pumping: a mechanism causing vertical transport of contaminated gases through fractured permeable media, J. Geophys. Res. Solid Earth 96 (1991) 21933–21948, https://doi.org/10.1029/91JB01836.
[5] O.N. Forde, A.G. Cahill, R.D. Beckie, K.U. Mayer, Barometric-pumping controls fugitive gas emissions from a vadose zone natural gas release, Sci. Rep. 9 (2019) 1–9, https://doi.org/10.1038/s41598-019-50426-3.
[6] H. Li, H. Zhan, X. Wang, Q. Guo, W. Liu, Y. Li, Y. Gong, Effect of earth–air breathing on evaporation of deeply buried phreatic water in extremely arid regions, Hydrol. Process. 35 (2021) e14078, https://doi.org/10.1002/hyp.14078.
[7] H. Li, F. Wu, H. Zhan, F. Qiu, W. Wang, The effect of precipitation pulses on evaporation of deeply buried phreatic water in extra-arid areas, Vadose Zone J. 15 (2016) 1–11, https://doi.org/10.2136/vzj2015.09.0127.
[8] H. Li, Y. Gong, S. Wang, Q. Guo, The effect of earth-air passive exchange on the formation of haze patterns, Environ. Earth Sci. 80 (2021) 1–12, https://doi.org/10.1007/s12665-021-09962-3.
[9] J.M. Terrones-Saeta, J. Suárez-Macías, F.J.L. del Río, F.A. Corpas-Iglesias, Study of copper leaching from mining waste in acidic media, at ambient temperature and atmospheric pressure, Minerals 10 (2020) 873, https://doi.org/10.3390/min10100873.

[10] L. Xu, X. Lin, J. Amen, K. Welding, D. McDermitt, Impact of changes in barometric pressure on landfill methane emission, Global Biogeochem. Cycles 28 (2014) 679–695, https://doi.org/10.1002/2013GB004571.

[11] S. Qi, Y. Wang, L. Wang, J. Luo, D. Hou, Impact of atmospheric pressure fluctuations on nonequilibrium transport of volatile organic contaminants in the vadose zone: experimental and numerical modeling, Water Resour. Res. 57 (2021) e2020WR029344, https://doi.org/10.1029/2020WR029344.

[12] E. Levintal, M.I. Dragila, H. Zafrir, N. Weisbrod, The role of atmospheric conditions in CO_2 and radon emissions from an abandoned water well, Sci. Total Environ. 722 (2020) 137857, https://doi.org/10.1016/j.scitotenv.2020.137857.

[13] S. Bourret, E. Kwicklis, T. Miller, P. Stauffer, Evaluating the importance of barometric pumping for subsurface gas transport near an underground nuclear test site, Vadose Zone J. 18 (2019) 1–17, https://doi.org/10.2136/vzj2018.07.0134.

[14] Y. Ganot, M.I. Dragila, N. Weisbrod, Impact of thermal convection on CO_2 flux across the earth–atmosphere boundary in high-permeability soils, Agric. For. Meteorol. 184 (2014) 12–24, https://doi.org/10.1016/j.agrformet.2013.09.001.

[15] S.N. Lyman, H.N. Tran, M.L. Mansfield, R. Bowers, A. Smith, Strong temporal variability in methane fluxes from natural gas well pad soils, Atmos. Pollut. Res. 11 (2020) 1386–1395, https://doi.org/10.1016/j.apr.2020.05.011.

[16] M. Moya, E.P. Sánchez-Cañete, R. Vargas, A. López-Ballesteros, C. Oyonarte, A.S. Kowalski, P. Serrano-Ortiz, F. Domingo, CO_2 dynamics are strongly influenced by low frequency atmospheric pressure changes in semiarid grasslands, J. Geophys. Res. Biogeosciences. 124 (2019) 902–917, https://doi.org/10.1029/2018JG004961.

[17] J. Feldman, M. Paul, G. Xu, D.X. Rademacher, J. Wilson, T.M. Nenoff, Effects of natural zeolites on field-scale geologic noble gas transport, J. Environ. Radioact. 220 (2020) 106279, https://doi.org/10.1016/j.jenvrad.2020.106279.

[18] C. Johnson, C.E. Aalseth, T.R. Alexander, T.W. Bowyer, V. Chipman, A.R. Day, S. Drellack, J.E. Fast, B.G. Fritz, J.C. Hayes, others, Migration of noble gas tracers at the site of an underground nuclear explosion at the Nevada National Security Site, J. Environ. Radioact. 208 (2019) 106047, https://doi.org/10.1016/j.jenvrad.2019.106047.

[19] J. Amaré, I. Bandac, A. Blancas, S. Borjabad, S. Buisán, S. Cebrián, D. Cintas, I. Coarasa, E. García, M. Martínez, others, Long term measurement of the ^{222}Rn concentration in the canfranc underground laboratory, Eur. Phys. J. C 82 (2022) 891, https://doi.org/10.1140/epjc/s10052-022-10859-z.

[20] J.L. Burnett, T.L. Stewart, M.E. Keillor, J.H. Ely, Investigating the detection of underground nuclear explosions by radon displacement, J. Environ. Radioact. 229 (2021) 106541, https://doi.org/10.1016/j.jenvrad.2021.106541.

[21] S. Chowdhury, A. Deb, C. Barman, M. Nurujjaman, D.K. Bora, Simultaneous monitoring of soil ^{222}Rn in the Eastern Himalayas and the geothermal region of eastern India: an earthquake precursor, Nat. Hazards 112 (2022) 1477–1502, https://doi.org/10.1007/s11069-022-05235-9.

[22] H. Li, W. Liu, H. Zhan, S. Sun, X. Wang, S. Wang, F. Li, X. Wang, Effect of barometric pumping on relative humidity in the loessal soil of the loess Plateau, Geoderma 424 (2022) 116008, https://doi.org/10.1016/j.geoderma.2022.116008.

[23] H. Li, S. Wang, F. Li, Y. Gong, X. Wang, Passive breathing of earth-air: "fingerprint" evidence from moisture records, J. Geophys. Res. Atmos. 127 (2022) e2021JD036057, https://doi.org/10.1029/2021JD036057.

[24] M. Zhang, H. Zhang, Z. Zeng, Z. Li, X. Wang, The mechanisms of efflorescent disaster of wall-paintings in Mogao Grottoes, J. Lanzhou Univ. 1 (1995).

[25] Y. Zhang, Z. Yu, L. Wang, Q. Cui, B. Shui, S. Sun, A study on the soluble salts used in the Murals of Mogao Cave 196, Dunhuang Res. (2021) 148–155, https://doi.org/10.13584/j.cnmi.issn1000-4106.2021.01.020.

[26] G. Chen, Study on Salting Damage Analysis and Treatment of Wall Paintings at Mogao Grottoes, Lanzhou University, Dunhuang, 2016.

[27] Y. Zhang, J. Wang, H. Liu, X. Wang, A non-destructive approach using MatLab software for morphology analysis of ancient mural deterioration, Stud. Conserv. 62 (2017) 384–392, https://doi.org/10.1080/00393630.2016.1183864.

[28] H. Li, Mechanism of formation of efflorescence belts based on the earth-air activity, Sci. Conserv. Archaeol. 34 (2022) 117–123, https://doi.org/10.16334/j.cnki.cn31-162/k.20210202033.

[29] H. Li, W. Wang, H. Zhai, Qiu, Influence of environment factors on water evaporation in Dunhuang Mogao Grottoes, J. Arid Meteorol. 32 (2014) 940–946, https://doi.org/10.11755/j.issn.1006-76399(2014)-06-0940.

[30] N. Hao, Y. Wang, X. Wu, Y. Duan, P. Li, M. He, Real-time experimental monitoring for water absorption evolution behaviors of sandstone in Mogao Grottoes, China, Energies 15 (2022) 8504, https://doi.org/10.3390/en15228504.

[31] H. Li, W. Wang, H. Zhan, F. Qiu, Q. Guo, S. Sun, G. Zhang, The effects of atmospheric moisture on the mural paintings of the Mogao Grottoes, Stud. Conserv. 62 (2017) 229–239, https://doi.org/10.1080/00393630.2016.1148916.

[32] S. Yang, A Preliminary Study of the Moisture and Salt Distribution in the Cliff of Mogao Grottoes, Lanzhou University, 2009.

[33] X. Wang, M. Zhang, H. Zhang, Z. Zeng, Z. Yao, Z. Zhou, Engineering properties of surrounding rocks of Mogao Grottoes at Dunhuang, Chin. J. Rock Mech. Eng. 19 (2000) 756–761.

[34] F. Ye, W. Chen, X. Ling, J. Zhang, Z. Guo, Q. Guo, Study on the weathering characteristics of the yumen glutenite in the Mogao Grottoes in Dunhuang, J. Eng. Geol. 24 (2016) 1286–1293, https://doi.org/10.13544/j.cnki.jeg.2016.06.031.

[35] Q. Zhou, H. Li, D. Wang, Y. Wang, Temperature and humidity variations in Cave 108 of the Mogao Grottoes and what they indicate about moisture and heat sources of the cave, Sci. Conserv. Archaeol. 30 (2018) 51–60, https://doi.org/10.16334/j.cnki.cn31-1652/k.2018.03.007.

[36] S. Yang, X. Wang, Q. Guo, Q. Pei, A study of the salt distribution in the cliffs of the Dunhuang Mogao Grottoes, Dunhuang Res. 125–129 (2017), https://doi.org/10.13584/j.cnki.issn1000-4106.2017.04.014.

[37] M. Angeli, J.-P. Bigas, D. Benavente, B. Menéndez, R. Hébert, C. David, Salt crystallization in pores: quantification and estimation of damage, Environ. Geol. 52 (2007) 205–213, https://doi.org/10.1007/s00254-006-0474-z.

[38] W. Bi, Z. Yan, Z. Zhang, S. Yao, J. Zhang, X. Wang, Modeling and numerical simulation of heat and mass transfer in the cave wall of the Mogao Grottoes in China, Build, Environ. Times 201 (2021) 108003, https://doi.org/10.1016/j.buildenv.2021.108003.

[39] X. Duan, H. Sun, A report on the restoration of the alkalized murals in Cave 108 at Mogao Grottoes, Dunhuang Res. (1990) 92–94, https://doi.org/10.13584/j.cnki.issn1000-4106.1990.03.014.

[40] J. Wang, Z. Yan, X. Wang, Z. Zhang, R. Shang, W. Bi, Experimental research on mechanical ventilation system for Cave 328 in Mogao Grottoes, Dunhuang, China, Energ, Buildings 130 (2016) 692–696, https://doi.org/10.1016/j.enbuild.2016.08.086.